Int. J. Heat Mass Transfer. Vol. 24, pp. 475–490
Pergamon Press Ltd. 1981. Printed in Great Britain

0017-9310/81/0301-0475 $02.00/0

NUMERICAL SIMULATION OF TURBULENT TEMPERATURE FLUCTUATIONS IN LIQUID METALS

GÜNTHER GRÖTZBACH
Institut für Reaktorentwicklung, Kernforschungszentrum Karlsruhe,
Postfach 3640, D-7500 Karlsruhe, F.R.G.

(*Received* 27 *May* 1980)

Abstract—The method of direct numerical simulation is used to investigate temperature fluctuations in fully developed turbulent liquid metal flows. Subgrid scale models using one transport equation account for the turbulence not resolved by the finite difference grid. A special subgrid scale heat flux model for liquid metal flows is deduced together with a method of calculating the model coefficients. At very small Peclet numbers the temperatures become independent of model parameters.

Numerical results for the Nusselt number in plane channels and for radial temperature and eddy conductivity profiles in annuli agree with published data. Nusselt numbers determined numerically for annuli indicate that many empirical correlations overestimate the influence of the ratio of radii. The numerical results for the eddy conductivity profiles may be used to reduce these problems. The statistical properties of the temperature fluctuations simulated are within the scatter band of experimental data. The numerical results confirm Lawn's theory, giving reasonable heat flux correlation coefficients which depend only weakly on the problem marking parameters.

NOMENCLATURE

a, constant thermal diffusivity;
c_p, constant specific heat capacity;
C_T, subgrid scale heat flux coefficients;
D, channel width, $R_2 - R_1$;
E, turbulence energy, power spectral density;
${}^jF$, grid surface, $V/\Delta x_j$;
Nu, Nusselt number;
p, pressure;
Pe, Peclet number, $Re\,Pr$;
Pe^*, friction Peclet number, $Re^*\,Pr$;
Pr, Prandtl number, ν/a;
Pr_t, turbulent Prandtl number, $\varepsilon_m/\varepsilon_H$;
$\dot{q}$, radial heat flux;
$\dot{Q}$, specific volumetric heat source;
$R_{1,2}$, inner, outer wall radii (Fig. 1);
Re, Reynolds number, ${}^v\langle u_1\rangle 2D/\nu$;
Re^*, friction Reynolds number, u^*D/ν;
t, time;
T, temperature;
T^+, universal temperature, T/T^*;
T^*, heat flux temperature, $\dot{q}_w/(\rho c_p u^*)$;
tsd, typical relative standard deviation;
u_i, velocity component, indices refer to Fig. 1;
u^*, friction velocity, $\sqrt{(\tau_w/\rho)}$;
V, grid volume, $\Delta x_1\,\Delta x_2\,\Delta x_3$;
χ, ϕ, periodicity lengths, see Fig. 1;
Δx_i, grid widths;
y, wall distance, mostly $y = R - R_1$.

Greek symbols

δ_j, central finite difference operator;
ε, turbulence dissipation;
ε_H, eddy diffusivity for heat, $-\langle u_3' T'\rangle/\langle \partial T/\partial x_3\rangle$;
ε_m, eddy diffusivity for momentum, $-\langle u_3' u_1'\rangle/\langle \partial u_1/\partial x_3\rangle$;
ν, kinematic viscosity;
ρ, constant specific density;
γ_T, correction factor in the subgrid scale heat flux model, $\gamma_T \geq 1$;
τ, radial shear stress.

Indices

i,j, space indices, Fig. 1;
t, turbulent;
T, temperature;
w, wall.

Operator for any quantity Y

$\langle Y\rangle$, time mean value;
${}^v\langle Y\rangle$, channel volume mean value;
${}^v\bar{Y}$, mesh cell volume mean value, $\int_v Y\,\mathrm{d}v$;
${}^j\bar{Y}$, mesh cell surface mean value, $\int_{j_F} Y\,\mathrm{d}^jf$;
$\bar{Y}$, average over both walls, cart. $k = 0$, cyl. $k = 1$,

$$(Y_{w1}R_1^k + Y_{w2}R_2^k)/(R_1^k + R_2^k);$$

Y', fluctuating part of $Y' = Y - \langle Y\rangle$, and $Y' = Y - {}^j\bar{Y}$.

1. INTRODUCTION

WORKING conditions in heat generating fuel elements of liquid metal cooled fast breeder reactors extend from high Reynolds number turbulent flows for normal operation down to laminar flows in case of decay heat removal. Thus, the models used to calculate the detailed temperature fields within the fuel elements

must account for molecular and turbulent heat transports alike. Usually, statistical turbulence models are applied which are based on the Reynolds equations. In most cases the unknown turbulent heat fluxes are modeled by the eddy diffusivity concept. The experimental determination of the eddy diffusivity for heat (= eddy conductivity) ε_H is difficult, due to many problems associated with the use of liquid metals. The theoretical way of applying formulations for the turbulent Prandtl number $Pr_t = \varepsilon_m/\varepsilon_H$ suffers from the same problems, because the models have to be fitted against experimental data.

Even after recent publications on the subject of eddy conductivities in liquid metal flows there are still many open problems. In [1] a large number of experimental data are summarized for the Nusselt number Nu, the universal logarithmic temperature profile T^+ and for the turbulent Prandtl number. In the region where both the velocity and temperature profiles follow logarithmic laws, the data shows a constant turbulent Prandtl number depending neither on the wall distance y nor on the molecular Prandtl number Pr. This cannot be used for low Peclet number flows, because in this case, the conductive sublayer extends from the wall almost to the center of the channel. Consequently, there is no region of a logarithmic temperature profile. Reynolds [2] discusses and classifies 30 different methods of predicting turbulent Prandtl numbers. Some methodological problems become evident, for example, missing or wrong functional dependences on the wall distance, the molecular Prandtl number, or the Reynolds number. In the work by Dutt [3], some discrepancies are noted between experimental and theoretically predicted data, but doubts are thrown upon the experimental data. Thermal contact resistance, incomplete wetting and longitudinal conduction appear to be the main reasons. This may be confirmed using the publication by Lawn [4]. Lawn develops a spectral theory to predict turbulent temperature fluctuations in liquid metals. In attempting to check this theory by summarizing experimental data for the turbulent Prandtl number, for the turbulent heat flux, for the RMS value of temperature fluctuations and cross stream velocity fluctuations, and for the heat flux correlation coefficients, he had to conclude that many of the published data are in error because they show correlation coefficients greater than one.

In this work, the direct numerical simulation technique is used to calculate turbulent liquid metal flows in plane channels and annuli. The method is based on a finite difference formulation of the complete time dependent three-dimensional mass, momentum, and energy equations for the gross scale part of turbulence. The small scales, which are not directly resolved by the finite difference grid, are represented by special subgrid scale models. Such a method was firstly applied to the momentum transport in channels by Deardorff [5] for inviscid flows, and by Schumann [6] for flows at finite Reynolds numbers. This author developed a model which is also applicable to low Reynolds number flows and which includes heat transports at different Prandtl numbers [7, 8]. The subgrid scale model coefficients are calculated by the theory of isotropic turbulence. In the first part of this work the peculiarities of the model and of the theory to calculate the coefficients, which correspond to applications to low Prandtl numbers, are discussed. Then the model is applied to the simulation of liquid metal flows. The purpose of this work is to predict statistical data for temperature fluctuations in some exemplary flows. The results can be used for the development of statistical turbulence models. The numerical results, for example, confirm the spectral theory of Lawn cited above.

2. NUMERICAL SIMULATION METHOD

In this Section a brief description of the basic principles of the method of direct numerical simulation and of the computer model used is given. More details about the derivation and the numerical solution of the basic equations are found in [7, 8].

2.1. *Volume averaged basic equations*

The method of direct numerical simulation of turbulent flows is based on the complete three-dimensional non-stationary equations for the conservation of mass, momentum and heat. For application of finite difference schemes these basic equations are transformed to a finite difference form for the mesh cell averaged variables Y (Y any quantity) by formal integration over the volume $V = \Delta x_1 \Delta x_2 \Delta x_3$ of one mesh cell. When averaging partial space derivatives the Gaussian theorem leads directly to finite differences $\delta_j {}^j\bar{Y}$ for surface averaged values ${}^j\bar{Y}$, where j denotes the normal of the respective mesh cell surface ${}^jF$. The resultant averaged equations for mass, momentum and thermal energy read as follows (for simplicity, Cartesian coordinates are used here; actually, cylindrical coordinates are used in the computer code):

$$\delta_i {}^i\bar{u}_i = 0$$

$$\frac{\partial}{\partial t} {}^v\bar{u}_i = -\delta_j \overline{{}^j u_j u_i} - \delta_i {}^i\bar{p} + \delta_j \left(\frac{1}{Re^*} \overline{{}^j \frac{\partial u_i}{\partial x_j}} \right) \qquad i = 1,2,3 \quad (1)$$

$$\frac{\partial}{\partial t} {}^v\bar{T} = -\delta_j \overline{{}^j u_j T} + \delta_j \left(\frac{1}{Pe^*} \overline{{}^j \frac{\partial T}{\partial x_j}} \right) + \dot{Q}.$$

The summation convention is used for repeated lower indices. These equations are made dimensionless by means of the channel width D, the friction velocity $\overline{u^*}$ averaged over both walls, the time scale $t^* = D/\overline{u^*}$, and the heat flux temperature $\overline{T^*} = \dot{q}_w/(\rho c_p \overline{u^*})$. Consequently, the Reynolds number is defined as $Re^* = \overline{u^*} D/\nu$, and the Peclet number is defined as $Pe^* = Re^* Pr$. $\dot{Q}$ is the specific volumetric heat source.

In the TURBIT-2 computer code [7] applied here the partial derivatives which still remain in equation (1), and the quantities not defined on the staggered grid used are approximated in a linear manner. For time integration an explicit mixed Euler leap frog scheme is used in combination with Galilean transformations of the mean velocity and temperature fields to maximize the permissible time step widths. The calculation of the pressure field follows the well-known method of solving a Poisson equation by means of the fast Fourier transformation.

The geometries modeled in the computer program are infinite plane channels and annuli with different radius ratios R_1/R_2. The infinity is due to the periodicity of the velocity and temperature fields in the mean flow direction x_1 and spanwise direction x_2. The periodicity lengths $X_1 = IM\Delta x_1$ and $X_2 = JM\Delta x_2$ (see Fig. 1) are prescribed via the corresponding numbers of mesh cells IM and JM, and via the respective grid widths Δx_1 and Δx_2. Due to periodicity, axial gradients in the temperature field cannot be recorded easily. A possible transformation is given in [7], but is not used here.

The wall conditions are mostly formulated exactly. Important exceptions are the wall shear stress

$$\tau_w = -1/Re^* \, \overline{\partial u_1/\partial x_3}^{3}$$

and the normal wall heat flux

$$\dot{q}_w = -1/Pe^* \, \overline{\partial T/\partial x_3}^{3}.$$

In turbulent channel flows with $Pr \geq 0.7$, both gradients show strong changes near the wall which cannot be resolved with the grids used. Therefore these wall fluxes are approximated consistent with the universal velocity and temperature profiles. The method accounts for influences of the wall roughness, Reynolds number, and grid resolution capabilities. For liquid metal flows no wall functions need to be used for the wall heat flux because of the large spatial extension of the conductive sublayer, which is directly resolved by the grids used. Thus, a valid approximation of the wall heat flux in case of liquid metal flows is

$$\dot{q}_w = -\frac{1}{Pe^*}\overline{\frac{\partial T}{\partial x_3}}^{3} \sim \frac{-2}{Pe^* \Delta x_3}(\overline{T}^{v}_{1} - T_w) \qquad (2)$$

where $\overline{T}^{v}_{1}$ is the temperature in the grid cell adjacent to the wall and T_w is the wall temperature.

2.2. *Subgrid scale heat flux model for liquid metals*

2.2.1. *Formulation of subgrid scale heat fluxes.* The basic equations (1) contain averaged products of velocities and temperature. In a first step we split the unknown terms by splitting the dependent variables in a large scale part $\overline{Y}^{j}$ directly resolved by the grid and in a subgrid scale part Y', which represents the unresolved fluctuating part of $Y = \overline{Y}^{j} + Y'$. This yields these equations, which are still accurate:

$$\overline{u_j u_i}^{j} = \overline{u_j}^{j}\,\overline{u_i}^{j} + \overline{u_j' u_i'}^{j}$$

$$\overline{u_j T}^{j} = \overline{u_j}^{j}\,\overline{T}^{j} + \overline{u_j' T'}^{j}. \qquad (3)$$

Only for the subgrid scale parts must model assumptions be introduced. The models used in the code have been described, and extensively tested over a wide range of Reynolds numbers, Prandtl numbers, ratios of radii, and space dependent wall roughnesses [7–9]. Here emphasis is put on the discussion of the strong influence of molecular conduction on the subgrid scale heat flux model in case of liquid metal flows. The model for such flows is the following:

$$\overline{u_j' T'}^{j} = -{}^{j}a_t \delta_j(\overline{T}^{v} - \langle \overline{T}^{v} \rangle) \qquad (4a)$$

$$j = 1, 2, 3.$$

$${}^{j}a_t = C_{T2}\,{}^{j}C_T({}^{j}F\,\overline{E'}^{j})^{1/2} \qquad (4b)$$

This means that we assume gradient diffusion proportional to effective eddy conductivities ${}^{j}a_t$ and to local gradients of the temperature fluctuations. The eddy conductivities are modeled by a kind of Prandtl-energy–length-scale model. The length and energy scales chosen account for the fact that the influence of the model tends to become zero with increasing spatial resolution. The characteristic length scale is ${}^{j}F^{1/2}$. The characteristic energy scale is the subgrid scale kinetic energy $\overline{E'}^{j}$ within the area ${}^{j}F$:

$$\overline{E'}^{j} = \frac{1}{2}\overline{(u_i - \overline{u_i}^{i})^2}^{j}. \qquad (5)$$

This energy is also used in the momentum subgrid scale model. It is calculated from an additional conservation equation which is solved simultaneously with equation (1).

2.2.2. *Calculation of model coefficients.* The coefficient ${}^{j}C_T$ in equation (4b) is introduced to correct for geometrical anisotropies of the grid. It depends only on grid parameters and is of the order one; in case of isotropic mesh cells, ${}^{j}C_T = 1$. The coefficient dominating in our special application is C_{T2}. It has to be determined so that the production of subgrid scale temperature variances caused by this model

$$\text{production} = \langle \overline{\overline{u_j' T'}^{j}\,\delta_j\,\overline{T}^{j}}^{j} \rangle \qquad (6)$$

is equal, in the statistical mean, to its subgrid scale dissipation $\overline{\varepsilon_T'}^{v}$:

dissipation =

$$\langle \overline{\varepsilon_T'}^{v} \rangle = \langle \overline{\varepsilon_T}^{v} \rangle - \langle \frac{1}{Pe^*}\overline{\delta_j \overline{T}^{j}\,\delta_j \overline{T}^{j}}^{j} \rangle \qquad (7)$$

These equations are taken from a formally deduced conservation equation for the subgrid scale temperature variances. The overbar $\overline{}^{j}$ denotes linear averaging over two neighbouring values in the j direction. From equations (4), (6) and (7) one gets:

$$C_{T2} = \frac{\langle {}^{v}\overline{\varepsilon_T} \rangle - \langle \frac{1}{Pe^*} \overline{\delta_j {}^{j}\overline{T}\ \delta_j {}^{j}\overline{T}} \rangle}{\langle {}^{j}C_T^2\, {}^{j}F\, \overline{{}^{j}\overline{E'}} \rangle^{1/2} \langle \overline{\delta_j {}^{j}\overline{T}\ \delta_j {}^{j}\overline{T}} \rangle \gamma_T} \tag{8}$$

The denominator has been split into two parts to replace the triple correlations, which introduces a correction factor γ_T of the order one ($\gamma_T \geq 1$).

We may assume that subgrid scale turbulence, which is mostly associated with high wave numbers, is nearly independent of boundary conditions etc. and can therefore be regarded as locally isotropic. So, the theory of isotropic turbulence as given, for example, in [10] can be used to calculate all correlations contained in equation (8) on the basis of the well-known Kolmogorov spectrum for the kinetic energy of turbulence $E(k)$ and on the basis of the Batchelor spectrum for twice the energy of the temperature fluctuations $E_T(k)$:

$$\begin{aligned} E(k) &= \alpha \langle \varepsilon \rangle^{2/3} k^{-5/3} \\ E_T(k) &= \beta \langle \varepsilon \rangle^{-1/3} \langle \varepsilon_T \rangle k^{-5/3}. \end{aligned} \tag{9}$$

For the constants in the spectra we use $\alpha = 1.5$ and $\beta = 1.3$ determined in a literature review.

An approximate formula to estimate C_{T2} on the basis of equation (9) is given in [11]. The complete theory to calculate all terms contained in equation (8), and similarly for ${}^{j}C_T$, is very extensive and complicated [7]. Here we must use the complete theory, because all geometric details of the anisotropic grid and molecular conduction must be taken into account. In the following result the functions $f_i(\Delta x_j)$, which are of no special interest here, are of the order one and depend only on grid parameters:

$$C_{T2} = \frac{1 - \beta f_1(\Delta x_i)\, Pe^{*-1}\, V^{-4/9} \langle \varepsilon \rangle^{-1/3}}{\gamma_T \beta \alpha^{1/2} f_2(\Delta x_i)}. \tag{10}$$

The dissipation ε_T of temperature variances has cancelled out. The second terms of the numerators of equations (8) and (10) represent the dissipation in the temperature field resolved directly. These terms are important only in those cases in which the Peclet number and the mesh volume are small. This means that in cases in which the turbulent temperature fluctuations are almost totally contained in the large-scale structure resolved directly, the dissipation $\langle \varepsilon \rangle$ is an additional unknown. A useful approximation for turbulent channel flow purposes is deduced from the assumption of equality of production $= -\langle u_1' u_3' \rangle \partial \langle u_1 \rangle / \partial x_3$, and dissipation of kinetic energy. Application of the Prandtl mixing length model and universal logarithmic velocity profile furnishes:

$$\langle \varepsilon \rangle = (\kappa y)^2 \left| \frac{\partial \langle u_1 \rangle}{\partial x_3} \right|^3 = \frac{1}{|\kappa y|} \tag{11}$$

We use $\kappa = 0.4$ for the Karman constant. Equation (11) makes the subgrid scale coefficient C_{T2} [equation (10)] dependent on the wall distance y. A numerical evaluation of equations (9)–(11) is shown in Fig. 2 for an equidistant Cartesian grid with $\Delta x_1 = \Delta x_2 = 1/8$ and $\Delta x_3 = 1/16$, later denoted grid K7. In accordance with the higher turbulent temperature fluctuations near the wall, and the correspondingly larger extension of the spectra of the temperature fluctuations to higher wave numbers, the model shows increasing values of C_{T2} for decreasing wall distance and for increasing Prandtl number.

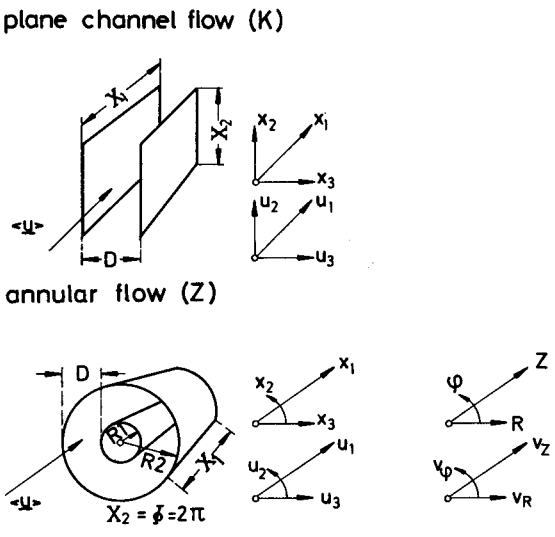

FIG. 1. Channel geometries under consideration. In both channels the time mean flow vector $\langle \mathbf{u} \rangle$ points in the x_1-direction.

The correction factor γ_T included in equation (8) must be determined empirically. In a sensitivity study it was tried in [7, 8] to adjust γ_T by using the coarse K7 grid for the simulation of a high-Reynolds number flow with $Pr = 0.7$; this is a case in which the subgrid scale heat flux model should be important. Nevertheless, γ_T showed very weak influences only. The high insensitivity to changes in γ_T is even more pronounced for lower Prandtl numbers. In Fig. 3, some results for five simulations of the flow of liquid sodium with different γ_T are shown. Theoretically, one expects $\gamma_T \geq 1$. For this range, almost no influence can be detected, although γ_T extends over two orders of magnitude and the coefficients C_{T2} are equal to zero only in the inner third of the channel. In order to use an unchanged turbulent subgrid-scale Prandtl number, the same value $\gamma_T = 1.4$ was chosen for all Prandtl numbers as in the subgrid scale model for the momentum fluxes.

3. CASE SPECIFICATIONS AND INITIAL CONDITIONS

Several calculations with different Reynolds numbers chosen at random were carried out for a plane channel and an annulus (Table 1) with the Prandtl number of liquid sodium under reactor conditions ($Pr = 0.007$). The resulting Reynolds number Re is related to Re^* prescribed, the channel average of the calculated mean velocity ${}^{v}\langle u_1 \rangle$, and the friction coefficient c_f:

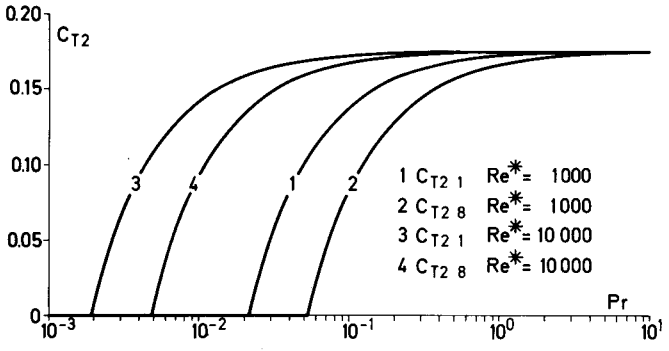

FIG. 2. Calculated coefficient C_{T2} ($\gamma_T = 1.0$) for grid $K7$ as a function of the Prandtl number. Parameters are the friction Reynolds number and the mesh index K in the x_3-direction [$y(K = 1) = 0.0313$ = mesh adjacent to the wall, $y(K = 8) = 0.469$ = mesh adjacent to the center].

$$Re^* = Re/(2^v\langle u_1\rangle) = Re/2\sqrt{(c_f/8)}. \quad (12)$$

The calculations of the flow of liquid mercury in an annulus, $Pr = 0.0214$, refer to the experiments by Dwyer *et al.* [12]. The calculations in air, $Pr = 0.7$ (1), have been added to show the steadiness of numerical results.

The thermal boundary conditions for the annuli are adiabatic outer walls and prescribed uniform wall heat fluxes at the heated inner walls. The plane channel flows of sodium are heated by volumetric heat sources within the fluid and cooled at the walls by prescribed uniform wall temperatures. These boundary conditions make the temperature profiles in the plane channels directly comparable to the profiles in uniformly cooled or heated pipes. The plane channel flow of air is cooled at wall $w1$ by a prescribed constant wall temperature, and heated at wall $w2$ by a constant heat flux.

To start the numerical time integration of equations (1), nearly arbitrary initial data for the three velocity components and for the temperature can be used; however, in order to shorten the computer time necessary to reach a fully developed flow we use the universal logarithmic laws for the mean of u_1 and T and zero for the mean of u_2 and u_3. A pseudo-random number generator is used to superimpose upon these mean values random fluctuations with amplitudes corresponding to the expected RMS-value profiles. Better initial data have been deduced for the case with $Pe = 350$, which uses the unchanged numerical results for the velocity fields of the case with $Pe = 35\,500$.

The parameters of the finite difference grids used are listed in Table 2. The Cartesian grids K use 2048 or 8192 mesh cells; the cylindrical grids Z use 4096 or 16384 mesh cells. The periodicity lengths Φ chosen for the circumferential direction in the annuli allow to record one quarter or half of the channel, which seems to be appropriate for the radius ratios under consideration [7]. The assignment to the cases of the given equidistant, but not equally sided, grids is shown in Table 1.

For the parameters of each case the radial profiles of all coefficients of the total subgrid scale model must be calculated. For example, the complete theory indicated in equations (8)–(11) leads to the results for C_{T2} listed in Table 3. For the three cases with the lowest Peclet numbers no subgrid scale heat flux model is necessary. As was to be expected from Fig. 2, increasing Peclet numbers make C_{T2} become non-zero, predominately near the walls, in annuli, especially near the outer walls. For the two highest Peclet numbers the subgrid scale heat flux coefficient is approximately constant all over the channels. For these two cases the complete subgrid scale heat flux model has been used as given in [7, 8], whereas the simpler model given in equation (4) has been used for all liquid metal flows.

Table 1. Case specifications. The grid specifications follow Table 2

Pr	Re	Pe	R_1/R_2	Grid	Thermal boundary conditions	$\dot{Q}$
0.007	46 000	322	0.25	Z9	$\dot{q}_{w1} = 1,\ \dot{q}_{w2} = 0$	0
	50 000	350	1.0	K2.2	$T_{w1} = T_{w2} = 0$	2
	100 000	700	0.25	Z2.2	$\dot{q}_{w1} = 1,\ \dot{q}_{w2} = 0$	0
	280 000	1960	1.0	K7	$T_{w1} = T_{w2} = 0$	2
0.0214	100 000	2140	0.479	Z2.2	$\dot{q}_{w1} = 1,\ \dot{q}_{w2} = 0$	0
	145 300	3110	0.479	Z2.2	$\dot{q}_{w1} = 1,\ \dot{q}_{w2} = 0$	0
0.7	50 000	35 000	0.25	Z2.2	$\dot{q}_{w1} = 1,\ \dot{q}_{w2} = 0$	0
0.71	50 000	35 500	1.0	K2.2	$T_{w1} = 0,\ \dot{q}_{w2} = -1$	0

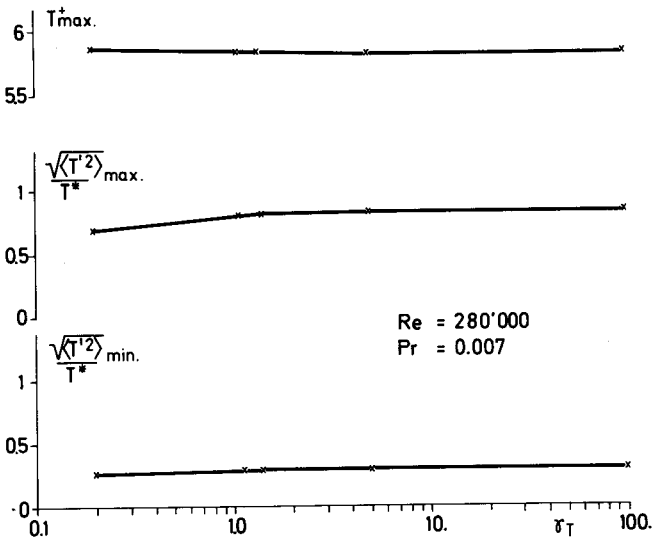

FIG. 3. Insensitivity of temperature results to changes of correction factor γ_T with grid $K7$; max. and min. are taken from the lateral profiles.

4. NUMERICAL RESULTS

Typical computer times for an IBM 370/168 and the numbers of time steps NT needed to reach fully developed flow and an additional time interval Δt_{av} for evaluation are given for each grid in Table 2 and for each case in Table 4. The channel lengths l covered are always greater than 50 channel widths, which is sufficient to reach fully developed flow.

4.1. *Phenomenological results*

Contour-line plots of the resolved instantaneous turbulent temperature fluctuations are shown in Fig. 4 for different annular flows with different molecular Prandtl numbers. The isolines show larger temperature fluctuations near the lower heated wall than near the upper adiabatic wall. With increasing Prandtl number the amplitude of the fluctuations increases, and the location of its maximum moves closer to the wall. The patterns show a predominant inclination from the walls in the Z-direction of the mean velocity to the center of the channel. The spatial extension of these structures decreases with increasing Prandtl number. In case of liquid sodium, the dominant structures are much more spatially extended than the typical grid width.

The same behaviour can be detected in cross-sections perpendicular to the mean flow direction (Fig. 5). In addition, these sections seem to show mainly large scale structures in the centre of the channels, whereas the scales are smaller near the heated walls. Thus we find temperature fluctuations with higher wave numbers in the main productive region near the heated wall, and with lower wave numbers in the inner part of the channel. This qualitative result agrees with the importance of the temperature subgrid scale model as given by the theoretical result for C_{T2} in Table 3.

4.2. *Profiles of temperature statistics*

For quantitative evaluation of the time dependent numerical results mean values are taken as averages over planes parallel to the walls. In addition, these mean values have been averaged over 21 to 43 different time steps equidistantly distributed within the final time intervals Δt_{av} (Table 4). In the same table some results are included which were calculated from the velocity fields and used for normalization purposes. The calculated velocity and pressure fields are not verified in this work. Those results, which do not depend on the molecular Prandtl number, were verified in [7–9].

Table 2. Grid specifications and typical computing times. IM, JM and KM denote the number of mesh cells in the three space directions

Grid specifications	K7	K2.2	Z9	Z2.2
IM (x_1, Z)	16	32	16	32
JM (x_2, φ)	8	16	16	32
KM (x_3, R)	16	16	16	16
X_1	2	3.2	2	3.2
X_2, Φ	1	2	$\pi/2$	π
Number of time steps	2690	1875	3080	2625
CPU-time, IBM 370/168	47 min	2.5 h	2 h	7 h

Table 3. Results for $C_{T2}(K)$ for mesh cell No. $K = 1$ near the wall w_1, for $K = 8$ near the center of the channel, and for $K = KM$ near the wall w_2. The calculated values are divided by $\gamma_T = 1.4$

Pr	Pe	Grid	$C_{T2}(1)$	$C_{T2}(8)$	$C_{T2}(KM)$	$C_{T2} = 0$ for $R - R_1)/(R_2 - R_1)$
0.007	322	$Z9$	0.0	0.0	0.0	0–1
	350	$K2.2$	0.0	0.0	0.0	0–1
	700	$Z2.2$	0.0	0.0	0.0	0–1
	1960	$K7$	0.067	0.0	0.067	0.31–0.69
0.0214	2140	$Z2.2$	0.065	0.0	0.079	0.44–0.5
	3110	$Z2.2$	0.081	0.030	0.090	—
0.7	35000	$Z2.2$	0.118	0.118	0.123	—
0.71	35500	$K2.2$	0.123	0.118	0.123	—

Table 4. Time intervals t with NT time steps, resultant channel mean velocities, covered channel lengths l, resultant wall shear stresses, distances y from the wall w_1 of zero turbulent shear stress, friction factors c_f, and number of time steps ΔNT_{av} within the final time intervals Δt_{av} used for time averaging

Pe	t	NT	$\frac{\langle u_1 \rangle}{u^*}$	$\frac{1}{D}$	$\frac{u_1^*}{u^*}$	$\frac{u_2^*}{u^*}$	$y\ (\tau = 0)$	c_f	ΔNT_{av}	Δt_{av}
322	3.16	3080	19.19	60.6	1.063	0.984	0.376	0.0217	28	1.16
350	8.24*	4225	19.36	159.5	1.0	1.0	0.5	0.0213	23	2.02
700	3.57	3875	20.93	74.7	1.072	0.981	0.376	0.0183	43	1.25
1960	6.97	2690	23.25	162.1	1.0	1.0	0.5	0.0148	21	2.69
2140	5.21	2450	20.88	108.8	1.037	0.982	0.432	0.0183	32	2.34
3110	20.4	9450	22.43	457.6	1.049	0.976	0.448	0.0159	30	3.24
35000	4.51	2625	19.61	88.4	1.071	0.981	0.376	0.0208	27	1.71
35500	4.00	1875	19.47	77.9	1.0	1.0	0.5	0.0211	22	1.56

*Restarted from case $Pe = 35500$ at $t = 4.0$ after initializing a new temperature field.

Cross stream profiles of temperature statistics evaluated from the plane channel flow simulations of liquid sodium are given in Fig. 6. All profiles are more or less symmetric to the center of the channel. The typical standard deviation *tsd* relative to local values is between 0.5 and 7% for the temperature RMS values and heat fluxes evaluated directly, and between 8 and 12% for the heat flux correlation coefficients and the eddy diffusivities for heat which by definition both are composed of different single results. The nearly parabolic temperature profiles are typical of conduction controlled flows. With increasing Reynolds or Peclet numbers the importance of turbulence increases. Accordingly, the RMS values of the turbulent temperature fluctuations and the turbulent heat flux $\langle u_3' T' \rangle$ become higher and the positions of the peaks move closer to the wall. The turbulent heat flux correlation coefficient shows nearly constant values in the outer parts of the channel with the higher Peclet number. In case of the lower Peclet number, the absolute value of the correlation coefficient increases as the walls are approached. The eddy diffusivity for heat increases with increasing Reynolds number. The maximum values, normalized by the thermal diffusivity a, confirm the very low contribution of the turbulent heat flux to the total flux in case of the lower Peclet number flow. Thus, both cases may be attributed to the transition range from molecular to turbulent heat transfer.

The results of the evaluation of the annular flow simulations are presented in Fig. 7. All profiles approach zero near the adiabatic outer wall. The radial heat flux correlation coefficients behave similarly, but there seems to be an indication of two approximately constant regions with different heights in the inner and outer halves of the channels. Again, the correlation coefficients for the lower Peclet numbers show a pronounced increase near the heated wall. The eddy diffusivity profiles are obviously not affected by the special thermal boundary conditions. The profiles show higher peaks near the outer wall, especially in case of the small ratios of radii of both low-Peclet number flows. The high-Peclet number profiles are not very different. It may be concluded that these results are near the limiting profile for high-Reynolds number flows of liquid mercury.

In addition to these evaluations of the numerical time and space dependent results a lot of evaluations of other correlations are possible, chiefly those mainly governed by the resolved large-scale structure of turbulence. Some examples included in [7] are the temperature–temperature, the energy–temperature, and the pressure–temperature cross correlations. A complete plot output from the computer code including velocity and pressure statistics is given in [13] for the annular flow with $Pe = 700$.

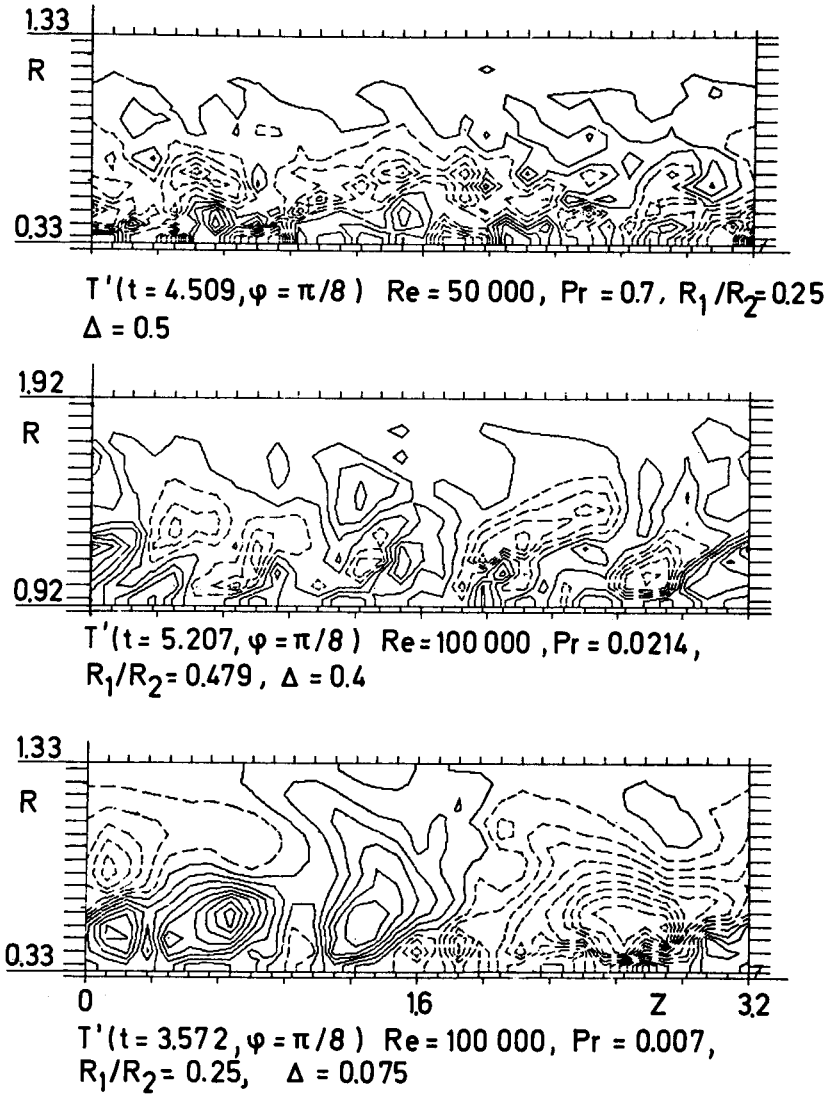

FIG. 4. Contour line plots of instantaneous resolved temperature fluctuations $T' = T - \langle T \rangle$ for annular flows of air, mercury, and liquid sodium. Sections along the mean flow direction Z. Δ = contour line increment. The dashed lines correspond to negative values.

5. DISCUSSION OF NUMERICAL RESULTS

To obtain an integral judgement on the simulated temperature fields we compare the evaluated Nusselt numbers in Fig. 8 with some empirical correlations taken from literature [14–18]. The numerical data of the plane channels, which have two non-adiabatic walls, agree with the respective formulae by Gräber [14] and Dwyer [15]. For the annular flows with adiabatic outer walls, the empirical data scatter widely, both as a function of the molecular Prandtl number and the ratio of radii. The correlation by Barthels [18] follows the numerical results for liquid mercury. The numerical results for liquid sodium flows, valid for a radius ratio of 0.25, are below most results of the correlations. The only curve which follows all numerical annular flow results, but gives slightly lower Nusselt numbers, is the curve by Gräber for a plane channel with one adiabatic wall. The large discrepancies between the empirical curves seem to be due to the problems in formulating radial eddy diffusivity profiles for annular channel flows. In plane channel flows no comparable difficulties appear, because the eddy diffusivity and eddy conductivity profiles may be approximated by using the direct analogy to pipe flows, which have been investigated more thoroughly.

A more detailed comparison of the numerical results with temperature profiles measured in an annular channel by Dwyer *et al.* [12] is made in Fig. 9. The temperature profiles are nearly identical. Due to the somewhat higher Reynolds number, the numerical results for the eddy conductivity profiles are also somewhat higher than the original and the smoothed

data calculated from the measured temperature profile by Dwyer *et al.* The typical standard deviation indicates comparable uncertainties in the numerical and the experimental results.

Some further results for the eddy conductivity have been plotted over the Peclet number in Fig. 10. In the log–log-presentation selected the plane channel data follow a single straight line, independent on the Reynolds and Prandtl numbers. The line is parallel to the line through the experimental pipe data found by Fuchs [19]. The distance between both lines corresponds to a difference in Peclet number by approximately a factor of two. The difference arises from the different numbers of thermal boundary layers in both channels. The data of the annular flows follow neither line: The eddy conductivity results for the mercury flows with $R_1/R_2 = 0.479$, which almost exactly follow the smoothed experimental data by Dwyer *et al.* [12], show a flatter increase with increasing Peclet number than the plane channel data, whereas the sodium flows with $R_1/R_2 = 0.25$ increase somewhat more steeply. All these results indicate the rather complicated influence on the eddy conductivity of the Reynolds number, Prandtl number, and of the radius ratio.

Also the advanced statistical turbulence models using additional transport equations for some turbulence quantities can be supported. By way of example, the peaks of the radial temperature RMS value profiles are plotted over the Peclet number in Fig. 11. The qualitative behaviour is largely comparable to that of the eddy conductivity. One important difference becomes evident from the numerical air flow results and from the experimental pipe data for air included in the figure. For constant Prandtl numbers the RMS values at large Peclet numbers are shown to depend not on the Reynolds number or on the Peclet number. At medium and low Peclet numbers the RMS-values seem to depend mainly on the Peclet number. Further influences arise from the radius ratio and from the thermal boundary conditions.

The experimental results for pipe flows [19–24]

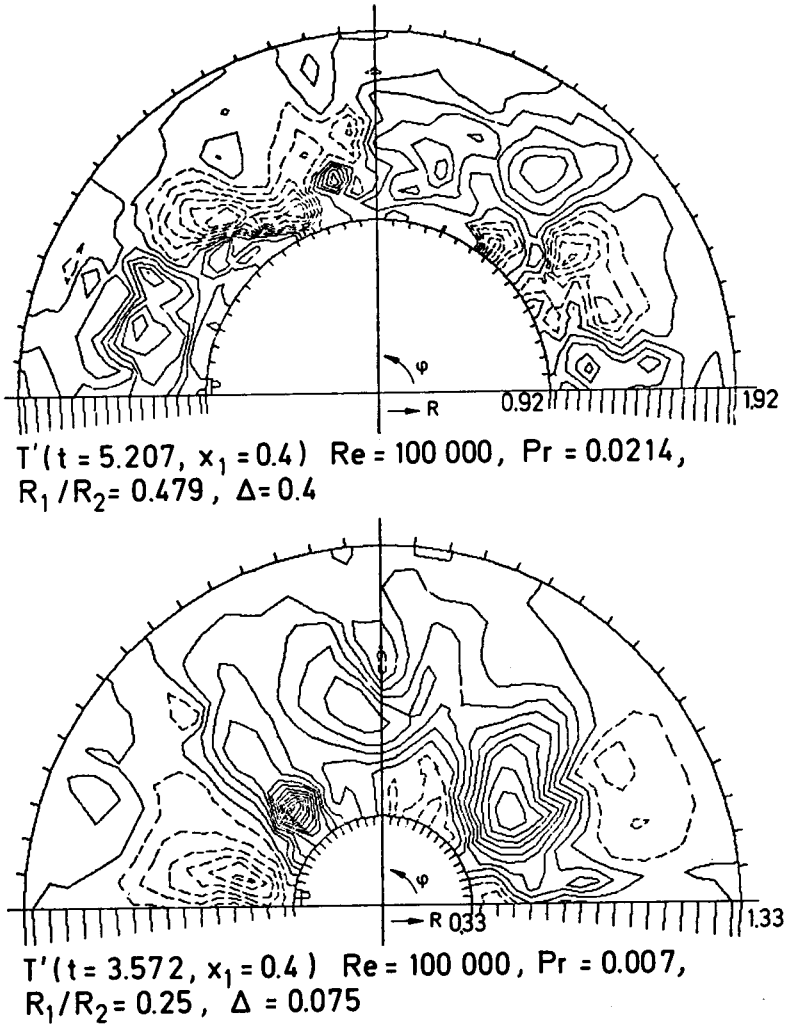

FIG. 5. Contour line plots of instantaneous resolved temperature fluctuations for annular flows of mercury and liquid sodium. Sections perpendicular to the mean flow direction.

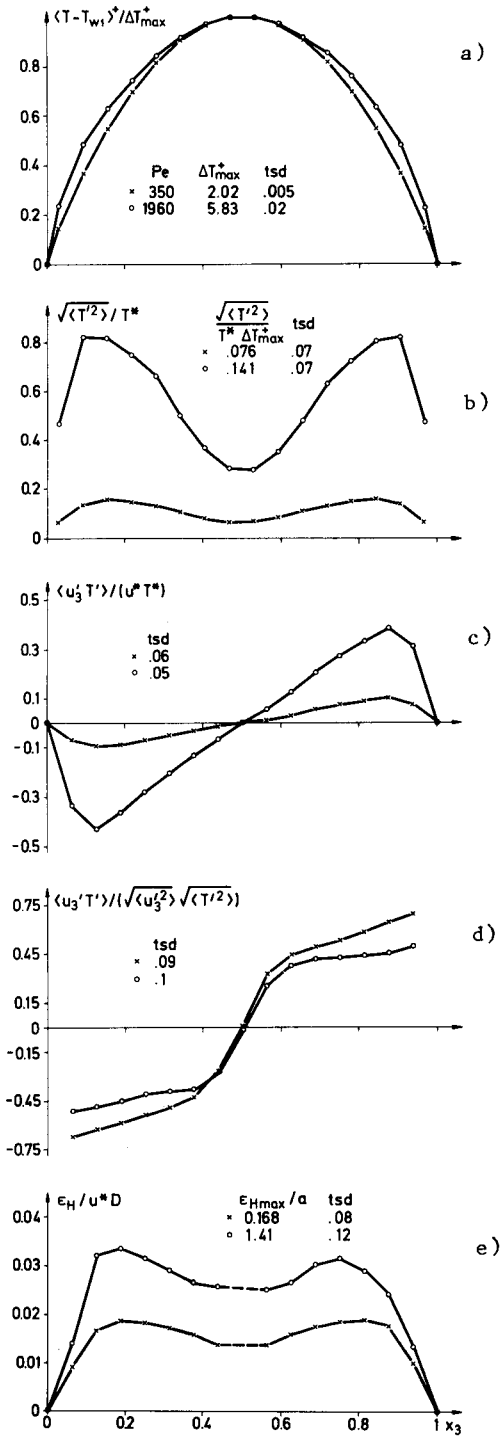

FIG. 6. Cross-stream profiles of temperature statistics for plane channel flows of liquid sodium. (a) Time mean temperatures normalized by $\Delta T^+_{max} = T^+_{max} - T^+_{W1}$; (b) resolved RMS-temperature values and (c) cross-stream turbulent heat fluxes; (d) heat flux correlation coefficients; (e) eddy diffusivities for heat.

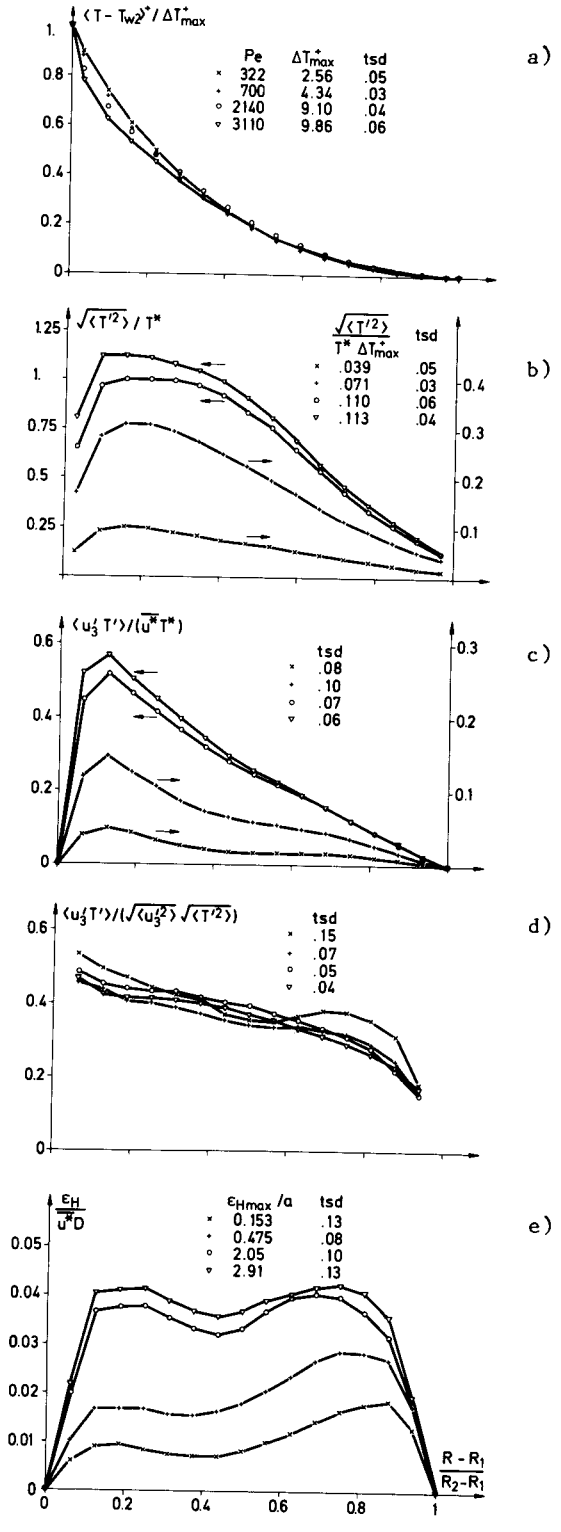

FIG. 7. Radial profiles of temperature statistics for annular flows of liquid sodium and liquid mercury. (a) Time mean temperatures; (b) resolved RMS temperature values and (c) cross-stream turbulent heat fluxes; (d) heat flux correlation coefficients; (e) eddy diffusivities for heat.

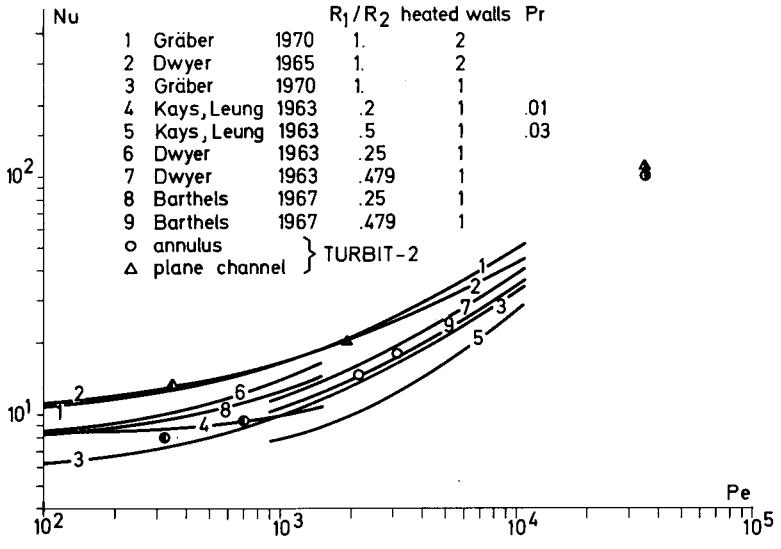

FIG. 8. Nusselt numbers $Nu = (\dot{q}_{conv} + \dot{q}_{cond})/\dot{q}_{cond}$ evaluated from numerical results and from empirical formulations. $^{v}\langle Pr_t \rangle = 1$ has been used for plotting some of the empirical curves. The Prandtl numbers of the numerical results are ▲, ◐, $Pr = 0.007$; ○, $Pr = 0.0214$; ▲, ◑, $Pr = 0.7(1)$.

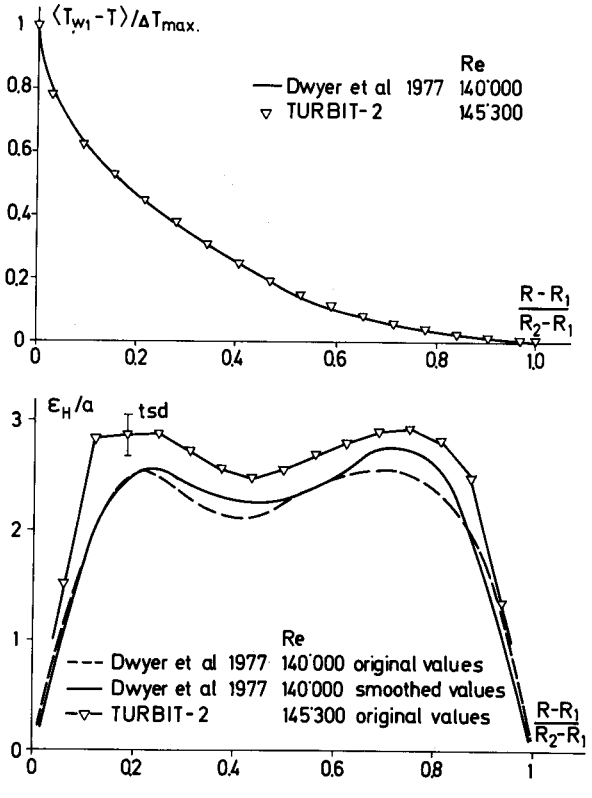

FIG. 9. Temperature and eddy conductivity profiles evaluated from the numerical simulation, case $Pe = 3110$, compared to measured and deduced annular flow data by Dwyer *et al.* [12].

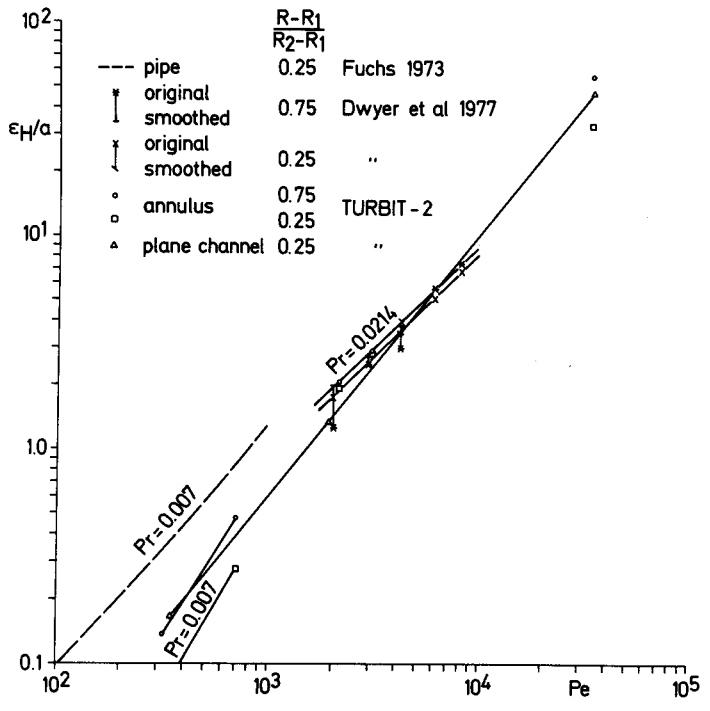

FIG. 10. Influence of Peclet number on the eddy conductivity normalized by the thermal diffusivity.

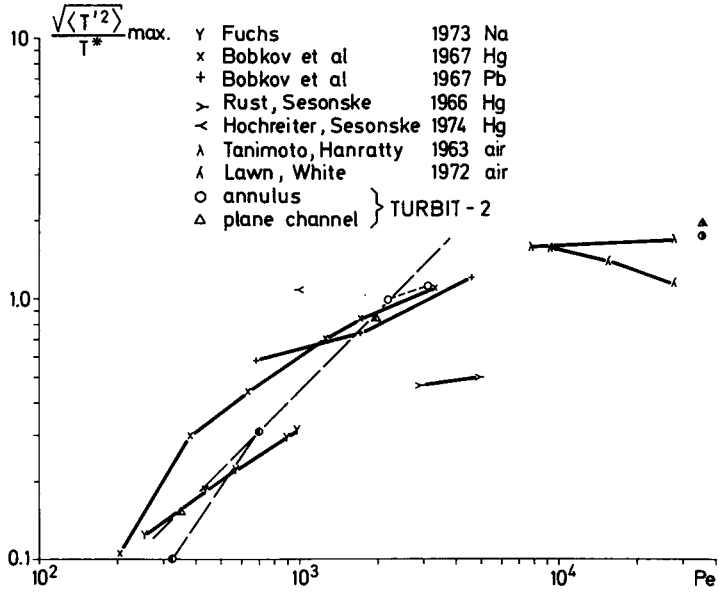

FIG. 11. Influence of Peclet number on the peaks of the radial temperature RMS-value profiles. All experimental data by [19–24] are for pipes. T^* used for normalization of Fuchs' data has been deduced from his data for T and T^+. For the symbols for the numerical results, see Fig. 8.

included in Fig. 11 scatter widely. This has also been found in the review by Lawn [4] for the RMS-values at a fixed point in the channel. The main reason for the scatter of the experimental data seems to be the limited frequency range of the sensors and the electronic equipment used [13]: For the Prandtl number of air, for example, the differences caused by slow sensors can be some 10 or 20% [8]. For the Prandtl number of liquid sodium the pipe data by Bunschi [25] permit the conclusion that the temperature RMS-values found by Fuchs [19] should be higher at least by 30% due to the high frequency cutoff used. Another open problem is the low frequency cutoff used in these experiments.

The discussion of these uncertainties of experimental temperature fluctuation results indicates why Lawn [4] was unable to verify his spectral theory in calculating the heat flux correlation coefficient. The corresponding experimental results scatter widely, because they contain the uncertain RMS temperature fluctuations. While Lawn cites values for the correlation coefficient (at $y = 0.25$) between 0.15 and 2.3, the numerical data at the position of the maximum RMS temperature values, taken from Figs. 6 and 7 and gathered in Fig. 12, are around 0.45. The numerical results show a uniform decrease for each Prandtl number with increasing Peclet number. This decrease is mainly due to volume averaging of the basic equations [equation (1)] over finite grid volumes: the sharp peak of the heat flux correlation coefficient very close to the wall, close to the outer edge of the conducting sublayer is not resolved by the grids used for air flows, but is partly resolved for the liquid metal flows with small Peclet numbers (Figs. 6 and 7). The correlation coefficients react even less sensitively to changes in the Peclet number in the inner parts of the channels. Thus, the numerical data confirm the results of Lawn's theory that the heat flux correlation coefficient is, if at all, a weak function of the Peclet number, except for the very low Peclet number cases with $\varepsilon_H/a < 1$ for which the convective turbulent heat flux is insignificant compared with the pure conductive heat flux.

6. CONCLUSIONS

The method of direct numerical simulation was applied in calculating turbulent liquid metal flows together with a theory to compute all coefficients of the subgrid scale models. The numerical results for the temperature fields react very insensitively to changes in the coefficients for the subgrid scale heat flux model determined theoretically. The temperature fluctuation fields resulting from the low Peclet number simulations do not depend on any coefficients in the temperature equations; qualitatively, the spatial structures in these fields follow the tendencies of the results for higher Peclet numbers, for which the subgrid scale heat flux model is relevant. The Nusselt numbers in plane channel flows, and some temperature and eddy conductivity profiles in annular flows, agree with published experimental data. From this we conclude that the theory of calculating subgrid scale coefficients furnishes adequate results over the whole range of Peclet numbers under consideration.

The turbulent heat flux data deduced from the numerical results indicate complex dependences on the Reynolds number, the Prandtl number, thermal boundary conditions and on the radius ratio. The large scatter of the empirical correlations for the Nusselt number in annular flows is mainly due to problems in formulating appropriate eddy conductivity profiles accounting for all cited parameters. The deduction of reasonable eddy conductivities or turbulent Prandtl numbers still remains an open problem for all liquid

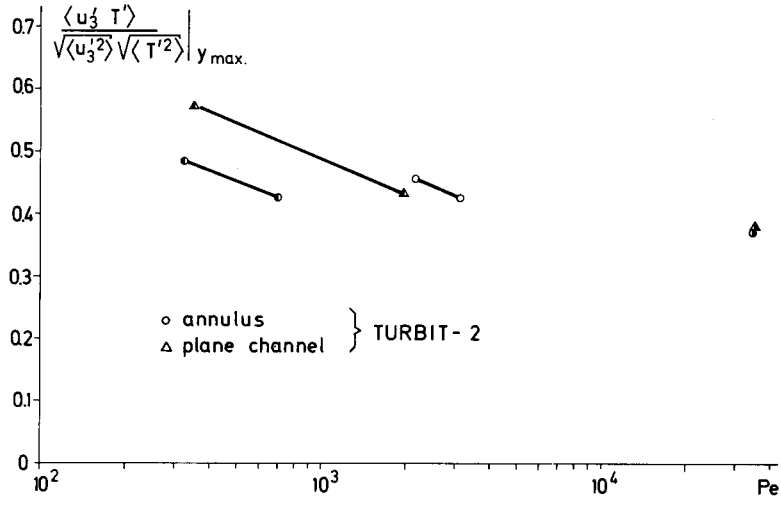

FIG. 12. Dependence of resolved radial heat flux correlation coefficient on the Peclet number at position y_{max} of the maximum of the RMS temperature values. Lines connect numerical results for cases with equal Prandtl numbers and radius ratios (for identification, see Fig. 8 and Table 1).

metal flows in annuli and other complicated channels. The eddy conductivity profiles for liquid metal annular flows derived numerically in this work are the first data in the literature to be determined directly. These results can partly support the development of models for the turbulent heat flux.

Existing statistical data on turbulent temperature fluctuations in liquid metal flows show large uncertainties. The main reason is the limited time resolution capability in most experiments. The numerical results for the RMS temperature fluctuations are within the range of experimental data; for low Peclet numbers, they show qualitatively comparable functional dependence on Reynolds number, Prandtl number, and radius ratio as the eddy conductivity. The radial heat flux correlation coefficient evaluated for all cases is close to most of the data published for air flows; it is a very weak function of the Peclet number. Thus, these numerical results confirm Lawn's theory.

REFERENCES

1. B. A. Kader and A. M. Yaglom, Heat and mass transfer laws for fully turbulent wall flows, *Int. J. Heat Mass Transfer* **15,** 2329–2351 (1972).
2. A. J. Reynolds, The prediction of turbulent Prandtl and Schmidt numbers, *Int. J. Heat Mass Transfer* **18,** 1055–1069 (1975).
3. N. V. K. Dutt, Turbulent heat transfer characteristics of liquid metals, *J. Scient. Ind. Res.* **36,** 165–171 (1977).
4. C. J. Lawn, Turbulent temperature fluctuations in liquid metals, *Int. J. Heat Mass Transfer* **20,** 1035–1044 (1977).
5. J. W. Deardorff, A numerical study of three-dimensional turbulent channel flow at large Reynolds numbers, *J. Fluid Mech.* **41,** 453–480 (1970).
6. U. Schumann, Subgrid scale model for finite difference simulations of turbulent flows in plane channels and annuli, *J. Comp. Phys.* **18,** 376–404 (1975).
7. G. Grötzbach, Direkte numerische Simulation turbulenter Geschwindigkeits-, Druck- und Temperaturfelder bei Kanalströmungen Diss., Universität Karlsruhe, Rep. KfK 2426 (1977).
8. G. Grötzbach and U. Schumann, Direct numerical simulation of turbulent velocity-, pressure- and temperature-fields in channel flows, *Symposium on Turbulent Shear Flows, Penn. St. Univ.*, 18–20 *April*, 1977, *Proc. Turbulent Shear Flows* I (edited by F. Durst *et al.*) pp. 370–385. Springer, Berlin (1979).
9. G. Grötzbach, Numerical investigation of the influence of secondary flows on characteristic turbulence data, KfK 2553 (1978).
10. J. O. Hinze, *Turbulence*, 2nd edn. McGraw-Hill, New York (1975).
11. U. Schumann, G. Grötzbach and L. Kleiser, Direct numerical simulation of turbulence, in *Prediction Methods for Turbulent Flows*, (edited by W. Kollmann) pp. 123–258. Hemisphere, New York (1980).
12. O. E. Dwyer, P. J. Hlavac and B. G. Nimmo, Eddy diffusivity of heat transfer in the radial direction for turbulent flow of mercury in annuli, *Int. J. Heat Mass Transfer* **20,** 141–151 (1977).
13. G. Grötzbach, Numerical simulation of turbulent liquid metal flows in plane channels and annuli, KfK 2968 (1980).
14. H. Gräber, Der Wärmeübergang in glatten Rohren, zwischen parallelen Platten, in Ringspalten und Längs-Rohrbündeln bei exponentieller Wärmeflußverteilung in erzungener laminarer oder turbulenter Strömung, *Int. J. Heat Mass Transfer* **13,** 1645–1703 (1970).
15. O. E. Dwyer, Heat transfer to liquid metals flowing turbulently between parallel plates, *Nucl. Sci. Engng* **21,** 79–89 (1965).
16. W. M. Kays and E. Y. Leung, Heat transfer in annular passages — hydrodynamically developed turbulent flow with arbitrarily prescribed heat flux, *Int. J. Heat Mass Transfer* **6,** 537–557 (1963).
17. O. E. Dwyer, On the transfer of heat to fluids flowing through pipes, annuli, and parallel plates, *Nucl. Sci. Engng* **17,** 336–344 (1963).
18. H. Barthels, Darstellung des Wärmeüberganges in konzentrischen Ringspalten unter Benutzung der Analogie zwischen Impuls- und Wärmeaustausch, Dissertation, Technische Hochschule Aachen, Rep. Jül-506-RB (1967).
19. H. Fuchs, Wärmeübergang an strömendes Natrium — Theoretische und experimentelle Untersuchungen über Temperaturprofile und turbulente Temperaturschwankungen bei Rohrgeometrie, Diss., Eidgen. Technische Hochschule Zürich, EIR-Bericht Nr. 241, Würenlingen (1973).
20. V. P. Bobkov, M. Kh. Ibragimov and V. I. Subbotin, Statistische Daten über turbulente Temperaturschwankungen in der Strömung, *Zh. Metally*, pp. 55–71. Moskau (1976). [German translation KfK-tr-372].
21. J. H. Rust and A. Sesonske, Turbulent temperature fluctuations in mercury and ethylene glycol in pipe flow, *Int. J. Heat Mass Transfer* **9,** 215–227 (1966).
22. L. E. Hochreiter and A. Sesonske, Turbulent structure of isothermal and nonisothermal liquid metal pipe flow, *Int. J. Heat Mass Transfer* **17,** 113–123 (1974).
23. S. Tanimoto and T. J. Hanratty, Fluid temperature fluctuations accompanying turbulent heat transfer in a pipe, *Chem. Engng Sci.* **18,** 307–311 (1963).
24. C. J. Lawn and R. S. White, The turbulence structure of heated pipe flow, CEGB Report RD/B/N 2159 (1972).
25. J. Bunschi, Turbulente Temperaturschwankungen im flüssigen Natrium, Diss., Eidgen. Technische Hochschule Zürich, Rep. AF-NST-13, Würenlingen (1977).

SIMULATION NUMERIQUE DES FLUCTUATIONS TURBULENTES DE TEMPERATURE DANS LES METAUX LIQUIDES

Résumé — On utilise la méthode de simulation numérique directe pour étudier les fluctuations de température dans les écoulements de métal liquide pleinement développés. Des modèles à échelle de sous-grille, utilisant une équation de transport, prennent en compte la turbulence non résolue par une grille aux différences finies. Un modèle spécial de flux de chaleur à sous-grille, pour les métaux liquides, est déduit avec une méthode de calcul des coefficients du modèle. Aux très petits nombres de Péclet, les températures deviennent indépendantes des paramètres du modèle.

Des résultats numériques pour le nombre Nusselt dans les canaux plats et pour les profils radiaux de température et de diffusivité turbulente dans les espaces annulaires s'accordent avec des données publiées. Les nombres de Nusselt déterminés numériquement pour les espaces annulaires indiquent que plusieurs formules empiriques surestiment l'influence du rapport des rayons. Les résultats numériques pour la conductivité turbulente peuvent être utilisés pour réduire ces problèmes. Les propriétés statistiques des fluctuations de température simulées sont dans la bande de dispersion des données expérimentales. Les résultats numériques confirment la théorie de Lawn en donnant des coefficients de corrélation de flux de chaleur raisonnables et qui dépendent seulement faiblement du problème des paramètres.

NUMERISCHE SIMULATION TURBULENTER TEMPERATURSCHWANKUNGEN IN FLÜSSIGMETALLEN

Zusammenfassung—Die Methode der direkten numerischen Simulation wird zur Untersuchung von Temperaturschwankungen in voll entwickelten turbulenten Flüssigmetallströmungen benutzt. Mit Feinstrukturmodellen, für die eine zusätzliche Transportgleichung gelöst wird, werden die nicht von den Maschennetzen aufgelösten Turbulenzanteile berücksichtigt. Die Koeffizienten des für Flüssigmetallströmungen vereinfachten Temperaturfeinstrukturmodells werden theoretisch bestimmt. Bei kleinen Peclet-Zahlen werden die berechneten Temperaturfelder unabhängig von Modell parametern.

Die numerisch bestimmten Nusselt-Zahlen für Plattenkanäle, und radialen Profile der Temperatur und der turbulenten Wärmeaustauschgröße für Ringspalte stimmen mit veröffentlichten Daten für die Fluide Natrium und Quecksilber überein. Die numerisch bestimmten Nusselt-Zahlen für Ringspalte deuten darauf hin, daß viele empirische Beziehungen den Einfluß des Radienverhältnisses überschätzen. Die berechneten Profile der turbulenten Wärmeaustauschgröße können zur Beseitigung dieses Problems benutzt werden. Statistische Eigenschaften der simulierten Temperaturfluktuationen befinden sich innerhalb der Streubänder experimenteller Daten. Die numerischen Ergebnisse liefern realistische Wärmestromkorrelationskoeffizienten, die zudem nur schwach von den Problemparametern abhängen; sie bestätigen damit die Theorie von Lawn.

ЧИСЛЕННОЕ МОДЕЛИРОВАНИЕ ТУРБУЛЕНТНЫХ ПУЛЬСАЦИЙ ТЕМПЕРАТУРЫ В ЖИДКИХ МЕТАЛЛАХ

Аннотация — Для исследования пульсаций температуры при полностью развитом турбулентном течении жидких металлов использован метод прямого численного моделирования. Поскольку для решения проблемы известные подсеточные модели, основанные на одном уравнении переноса, недостаточны, автором предложены специальная подсеточная модель теплопереноса в жидких металлах и метод вычисления модельных коэффициентов. При очень малых значениях числа Пекле температура перестает зависеть от параметров модели. Результаты численных расчетов числа Нуссельта для плоских каналов, а также профилей радиальной температуры и вихревой теплопроводности в кольцевых каналах согласуются с опубликованными данными. Значения числа Нуссельта, рассчитанные численным методом для кольцевых каналов, свидетельствуют о том, что многие из эмпирических соотношений переоценивают роль отношения радиусов. Данные численных расчетов профилей вихревой теплопроводности могут использоваться для более корректного учета влияния данного параметра. Статистические характеристики смоделированных пульсаций температуры не выходят за полосу разброса экспериментальных значений. Данные численных расчетов подтверждают результаты предложенного Лоуном модельного корреляционного описания теплопереноса в жидких металлах, дающие приемлемые значения коэффициентов корреляций для теплового потока.